Journal of Hydrology: Regional Studies 42 (2022) 101128

Contents lists available at ScienceDirect

Journal of Hydrology: Regional Studies

journal homepage: www.elsevier.com/locate/ejrh

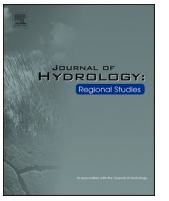

Dynamic multi-dimensional identification of Yunnan droughts and its seasonal scale linkages to the El Niño-Southern Oscillation

Linyan Zhang [a,b], Xiaoli Yang [a,b,*], Liliang Ren [a,b], Justin Sheffield [c], Linqi Zhang [a,b], Shanshui Yuan [d], Mengru Zhang [a,b]

[a] State Key Laboratory of Hydrology-Water Resources and Hydraulic Engineering, College of Hydrology and Water Resources, Hohai University, Nanjing 210098, China
[b] College of Hydrology and Water Resources, Hohai University, Nanjing 210098, China
[c] Geography and Environment, University of Southampton, Southampton, UK
[d] Yangtze Institute for Conservation and Development, Hohai University, Nanjing, Jiangsu, China

ARTICLE INFO

Keywords:
Drought
SAD method
SPI3
ENSO
Yunnan Province

ABSTRACT

Study region: Yunnan Province, China.
Study focus: Yunnan Province (YP) is affected by frequent droughts that severely affect local agriculture and the ecological environment. Therefore, the identification of droughts and an analysis of their driving factors are of significant importance for mitigating local drought losses and guiding agricultural practices. This study identified the spatiotemporal distribution and dynamic changes in drought events over YP (period 1961–2018) using the severity-area-duration method. The impact of El Niño-Southern Oscillation (ENSO) on seasonal droughts and their lag period were also quantified by employing the sliding correlation coefficient and cross-wavelet analysis method.
New hydrological insights for the region: 74 drought events were identified during 1961–2018 in YP, which were mainly short-duration that occurred in the 1980 s and 2000 s, and most drought centers are located over the northern and eastern parts of YP. We found that a significant correlation and different lag periods exist between Oceanic Niño Index (ONI) and seasonal precipitation in YP. Spring droughts mainly occurred in El Niño years during the 1980 s and the 1990 s, whilst winter droughts mainly occurred in La Niña years during the 1990 s and the 2000 s with a lag period of up to 12 months.

1. Introduction

Droughts are the most prominent natural hazards in China: complex, severe, and recurrent extreme climate events that occur anywhere and anytime, which differ from other disasters characterized by specific seasonal and regional distributions (Cheng et al., 2020; Hao and AghaKouchak, 2013; Su et al., 2021). The damages and losses caused by droughts are significantly greater than other natural hazards due to their wider spatial extent and longer influencing time (Ding and Gao, 2020; Ma et al., 2020); they significantly impact China's economy, agriculture, and environment (Liu et al., 2019; Zhang et al., 2021).

* Corresponding author at: State Key Laboratory of Hydrology-Water Resources and Hydraulic Engineering, College of Hydrology and Water Resources, Hohai University, Nanjing 210098, China.
E-mail address: yangxl@hhu.edu.cn (X. Yang).

https://doi.org/10.1016/j.ejrh.2022.101128

Available online 6 June 2022

Drought over Yunnan is affected by anthropogenic climate change (Wang et al., 2021). It experienced an overall drying trend (Liu et al., 2015; Wang et al., 2017; Hao et al., 2017), and is projected to increase in the warming future (Chen and Yuan, 2021). The annual and interannual variations of precipitation and temperature are significant changes in YP (Liu et al., 2014; Li et al., 2015a, 2015b). Droughts occur annually in YP, lasting for a long duration (more than 3 months) and prevailing over large areas, causing tremendous losses to agriculture, ecosystems, the economy, and social life (Yu et al., 2020; Li and Liu, 2011). Over the past 60 years, YP droughts are most likely to occur in winter, spring, and early summer; in particular, droughts with long duration and high severity mainly mostly occurred in the eastern and central of YP (Ma et al., 2013; Li et al., 2015a, 2019, 2015b). The Meteorological Disaster Record in China-Yunnan (MDRCY) indicated that the crop area affected by droughts in YP reached a total of 1,479,410,000 km^2 during 1950–1997, and about 50% of counties were affected by drought in varying degrees annually (Wen and Liu, 2006). However, there have been few explorations of the development process and path shifting of droughts in YP. Therefore, it is necessary to discuss the changing characteristics and path shifting of droughts in YP.

Droughts are generally identified and characterized using drought indices (Hao and Singh, 2015). The SPI, based on cumulative precipitation probabilities, is advantageous as it considers a range of timescales with stable frequencies of drought (Tayfur, 2021). It helps identify the onset and recovery of individual drought event relative to the PDSI, which is characterized by a single timescale and poor spatiotemporal comparability (Caloiero et al., 2018). In terms of drought characteristics, the severity, area, and duration are often identified by the time series of such drought indices (Zhai et al., 2016). However, the spatial extent of drought and how this evolves is an important aspect of the drought that is often not considered but needs to be taken into account to better characterize risks and drivers (He et al., 2020).

Andreadis et al. (2005) developed the severity-area-duration (SAD) method that provides a framework for identifying droughts considering their spatial and temporal dimensions. It combines the severity, area, and duration to analyze the drought characteristics over time (Yang et al., 2020a, 2020b). This method has been applied on global (Zhan et al., 2020; He et al., 2020) and regional scales (Wang et al., 2011; Liu et al., 2013; Zhai et al., 2016; Shao et al., 2018). Here we apply the SAD method for drought identification in YP that considers the continuity and dynamic changes in the spatial and temporal dimensions. The paths of drought centers also are displayed for further monitoring of the drought dynamic changes.

ENSO is a large-scale climate phenomenon affecting atmospheric and marine teleconnection (Liu et al., 2018). It is the strongest driver of interannual variation of tropical air-sea interactions, which significantly affects global climate (Philander, 1983; Yadav et al., 2013; Wanders et al., 2017; Torres-Valcarcela, 2018). The occurrence of droughts in lower latitudes is generally influenced by the interaction between the monsoons and ENSO events (Cheng et al., 2020; de Oliveira-Júnior et al., 2018; Zambrano Mera et al., 2018). Droughts in YP are closely linked to atmospheric circulation anomalies (Li et al., 2019), with a "lagged response" to ENSO. For example, Zhou et al. (2021) found that agricultural droughts were lagged relative to ENSO, as indicated by the correlation between

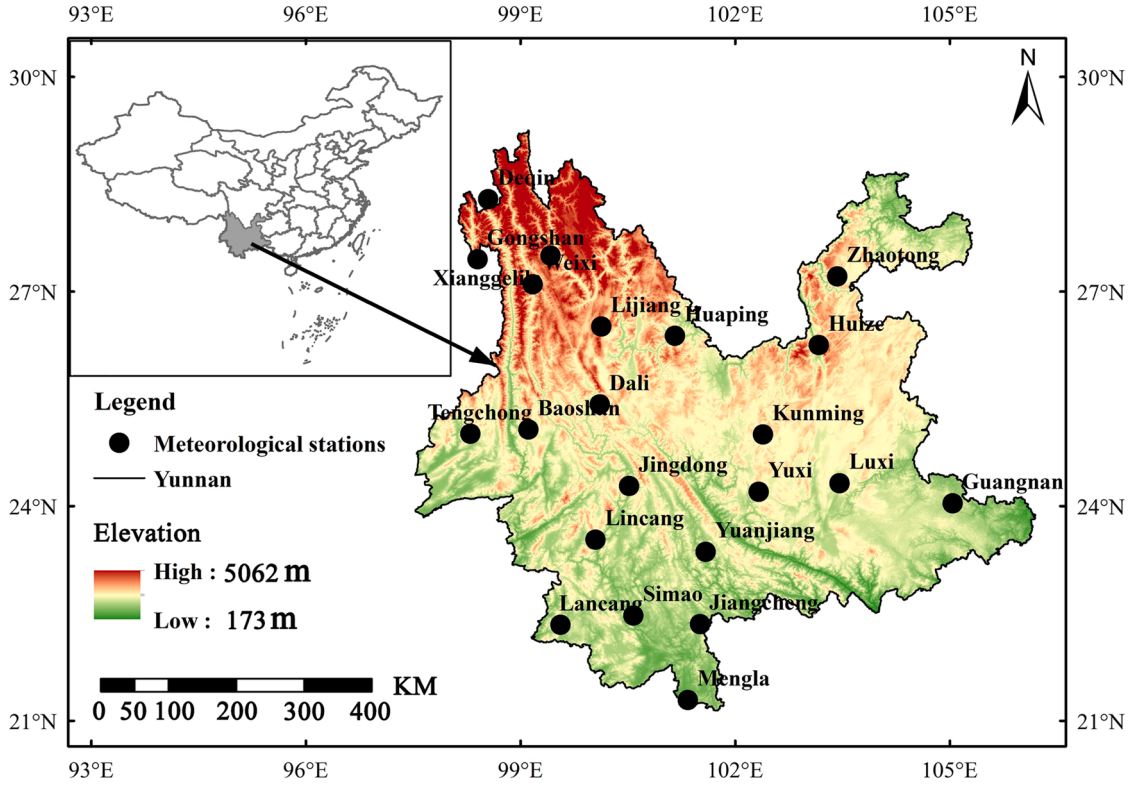

Fig. 1. The locational distribution of meteorological stations in the Yunnan Province.

climate and drought indices at 1–12 months. Also, Yao et al. (2019) discovered that hydrological droughts had a significant response to ENSO, with lags in sub-basins mostly around 8–9 months. However, there have been few explorations of the response of meteorological drought to ENSO in YP. Meanwhile, drought in southwest China has significant seasonal variations due to the joint influence of south Asia monsoon and ENSO events (Li et al., 2019; Cheng et al., 2020; Ding and Gao, 2020). Droughts occur more frequently in winter and spring than in other seasons (Wen and Liu, 2006; Ding and Gao, 2020), which caused great losses to Yunnan's agriculture and social economy. Research on the lagged impact of ENSO from the seasonality perspective is important for revealing the response period of seasonal droughts to ENSO and to inform the mechanisms of an early seasonal drought warning.

Therefore, this study aims to (1) employ the SAD method to identify drought events in YP, including quantifying their characteristics by using the 3-month SPI; (2) analyze their spatial and temporal dimensions, to understand dynamic changes in drought centers; and (3) explore possible multi-scale relationships including the seasonally lagged response between droughts and the ENSO.

2. Materials and methods

2.1. Study area

YP is to the Southwest of China (Fig. 1) with a land area of 394,100 km^2. It belongs to the low-latitude mountain plateau with a stepped distribution from north to south and has variable topography and landform (Yu et al., 2020). The province is strongly affected by the dry continental climate system in winter and the humid south Asian monsoon in summer (Cao et al., 2012) which leads to evident dry and rainy seasons (Hao et al., 2017; Song et al., 2019). As reported by the China Meteorological Disaster ceremony, the dry season (November to April of the subsequent year) accounts for only 16% of the annual precipitation and had a relatively higher drought frequency, broader range, and longer duration than those of the other provinces of China.

2.2. Datasets

Daily precipitation data from 22 meteorological stations were collected from the Chinese Meteorological Data Sharing Service (http://data.cma.cn/) (Fig. 1). To analyze the spatial characterization of droughts, precipitation data was interpolated into 10 km × 10 km spatial resolution using the inverse distance weighting method. YP area consisted of 4799 grid cells at this resolution. The monthly Oceanic Niño Index (ONI) and Southern Oscillation Index (SOI) from 1961 to 2018 were collected from the NOAA Earth System Research Laboratory (http://www.esrl.noaa.gov/). The ONI index was used to monitor the ENSO and was calculated as the 3-month running mean of sea surface temperature anomalies in the Niño 3.4 region (the range between 5°N–5°S and 120–170°W). The value of ONI at or exceeding + /- 0.5 °C and lasting for over 5 months was characterized as an El Niño/La Niña event (Table 3). The geopotential height at 500 hPa, horizontal and vertical wind at 850 hPa during 1961–2018 are collected from the NCEP/NCAR Reanalysis daily dataset with 2.5° × 2.5° resolution (https://psl.noaa.gov/data/gridded/data.ncep.reanalysis.pressure.html). It was collected to reveal the influence of large-scale circulation on the drought shifting path.

2.3. Methodology

2.3.1. Standardized precipitation index

The standardized precipitation index (SPI) considers a deficit of precipitation at different time scales (Mckee et al., 1993). This index is advantageous considering its flexible timescales and stable frequency for droughts, which makes up for the deficiencies of the PDSI, which is characterized by a single timescale and poor spatiotemporal comparability. The World Meteorological Organization (WMO) describes the SPI as a widely applied meteorological drought indicator, used in over 70 countries owing to its versatility. Among the various time scales of SPI, the SPI3 shows higher correlations between cropland exposed to drought and decreases in crop production than longer timescales (Udmale et al., 2020), and it is commonly used to reflect the surplus and deficit of moisture at short timescales (Scaini et al., 2015). Meanwhile, the 3-month scale of the drought indicator helps capture the length of the cropping season, for example, three to four months. Hence, the SPI3 was used here as the input dataset of the SAD method to analyze drought characteristics in YP.

2.3.2. SAD method for drought identification

Drought is a process involving continuous dry conditions with a certain duration and in a contiguous area (Zhai et al., 2016). The SAD method applies a simple clustering algorithm, based on the spatial proximity of grid cells that are in drought, to characterize the severity, areal extent, and duration of contiguous drought events (Yang et al., 2020a, 2020b). This study used a threshold of SPI3 less than − 1 to identify droughts. Spatially contiguous drought events can break up to form sub-droughts; furthermore, several droughts could merge into a larger drought across a specified minimum area (Sheffield et al., 2009). A suitable minimum area threshold of 150, 000 km^2 was selected for China (~1.5% of China's land area) according to Wang et al. (2011). Following this principle, we selected 6000 km^2 as the minimum threshold to identify drought events in YP, given the overall smaller area of YP.

Based on SPI3, severity (S) for each grid cell was calculated as:

$$S = 1 - \frac{\sum P}{t} \tag{1a}$$

$$P_i = \frac{SPI3_i - \min\limits_{1\le j\ll n}\{SPI3_j\}}{\max\limits_{1\le j\ll n}\{SPI3_j\} - \min\limits_{1\le j\ll n}\{SPI3_j\}} \tag{1b}$$

where here P_i is the standardized SPI3 of month i, $\sum P$ is the sum over for t months.

The grid cell with the maximum severity was identified as a drought center (Wang et al., 2011). The 3 × 3 neighborhood cells with the highest severities were added to the drought center and then averaged for both severities over the drought area. Stopped this process when there was no drought grid in the neighboring cells. The average severity of an event with different time intervals (3, 6, 9, 12, 15, and 18 months were selected based on the duration of droughts in YP) and areas (starting from 6000 km^2 to the maximum drought extent of approximately 39 ×10^4 km^2, in increments of 80 grid cells) were determined while identifying drought events. We identified the maximum severity event considering the interval and duration of each area based on the above procedure for calculating the SAD relationships for each drought event. SAD curves are constructed according to the average drought severity of different areas for a given duration (Andreadis et al., 2005). While, the SAD envelope curves were plotted by selecting the maximum severity of identifying events for the increment of each area, which reflects the most severe event for each combination of area and duration in various drought-affected areas (Yang et al., 2020a, 2020b).

2.3.3. *Correlation analysis and wavelet analysis*

Hudgins (1993) developed the cross-wavelet analysis, which is widely used to analyze the correlation between two time series across different time scales. It helps identify significant relationships between different time intervals and frequency bands (Torrence and Compo, 1998; Torrence andWebster, 1999). Therefore, we used this method to explore the correlation between climate indices (ONI and SOI) and SPI3. Meanwhile, the sliding correlation analysis method (Giovannettone and Zhang, 2019) was used to explore the seasonal variation in the relationship between the climate index (ONI) and precipitation. Assuming that $W_X(S)$ and $W_Y(S)$ are the wavelet transforms of X and Y time series respectively, the cross-wavelet spectrums of X and Y are defined as (Torrence and Webster, 1999):

$$W_n^{XY}(s) = W_n^X(s) \quad W_n^{Y*}(s) \tag{2}$$

where * denotes a complex conjugation and s is the stretching scale. A higher value of $W_n^{XY}(s)$ indicates a significant correlation between the two time series.

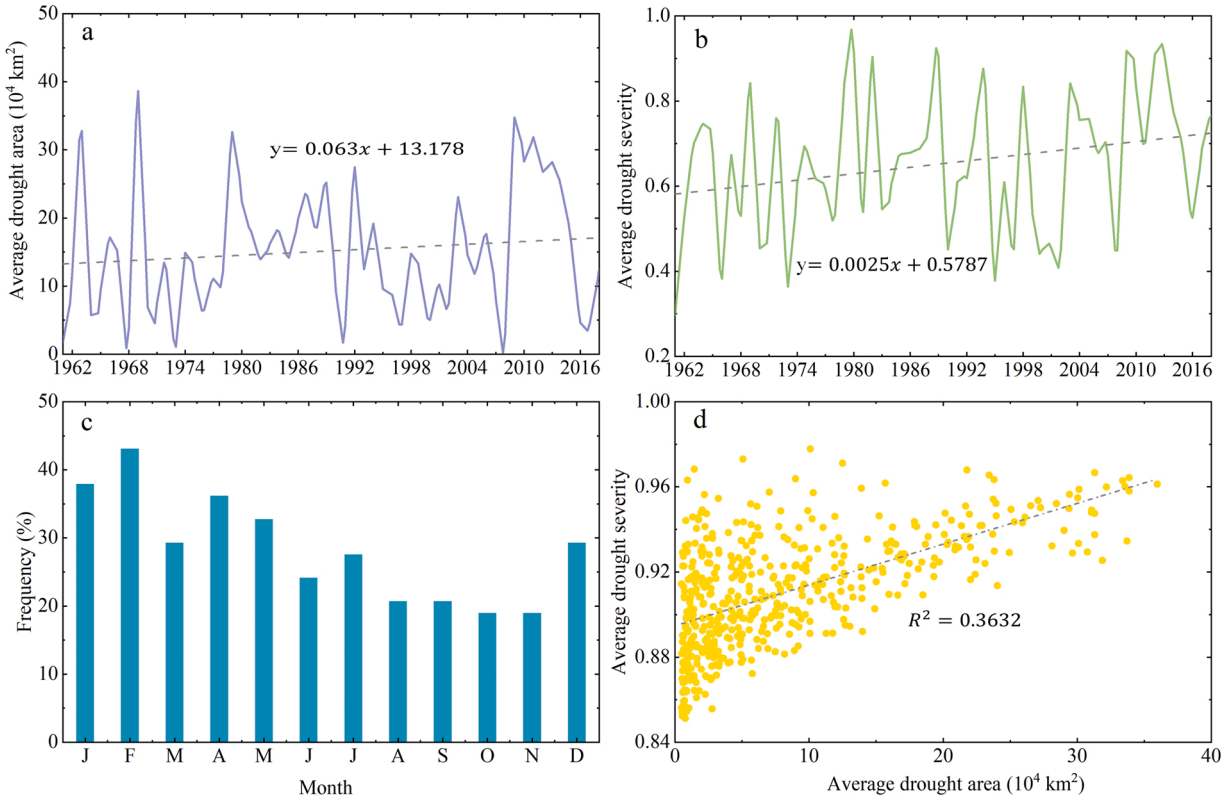

Fig. 2. Statistics for the annual average drought area (a), the annual average drought severity (b), the proportion of drought frequency (c), and the average severity and average drought area for each drought month (d).

The cross-wavelet power with the red noise power spectra P_K^X and P_K^Y can be expressed as follows:

$$\frac{\left|W_n^X(s) \quad W_n^{Y*}(s)\right|}{Q_X Q_Y} = \frac{Z_v(p)}{v}\sqrt{P_K^X P_K^Y} \tag{3}$$

where Q_X and Q_Y are the standard deviations of time series X and Y, while $Z_v(p)$ represents the confidence level about probability P with a probability distribution function.

3. Results

3.1. Drought characteristics of Yunnan Province

Fig. 2 shows the percentage of the annual average drought area, annual average severity, and drought frequency for each month in YP. During 1961–2018, 74 drought events were identified in YP. There are 44 droughts (60% of the total) with durations shorter than 6 months. The annual average severity and drought area showed an increasing trend in YP (Fig. 2(a and b)). The months from January to May had the highest drought frequency during 1961–2018 (Fig. 2(c)). Fig. 2(d) indicates that average severity increases with the increment of the drought area. As shown in Fig. 3, the average duration was longer in central and eastern YP, and the numbers of drought events were more in western and southern regions.

The onset month of the droughts primarily occurred in summer (Fig. 4), with approximately 12 droughts occurring in June. The end month of the droughts mostly occurred in autumn. Additionally, the droughts mainly started and ended in June during the 1960 s, 1980 s, 1990 s, and 2000 s; however, droughts in the 2010 s mostly started in March and April, which indicates that the drought onset months are getting earlier during study periods. In general, droughts occurred more frequently during 1980–2010 in YP and lasted for less than 12 months.

We compared the identified drought events using the SAD method with the recorded drought events in MDRCY (Table 1). The droughts in 1966, 1968/1969, 1974, and 1984 had the largest affected area. Meanwhile, those in 1968/1969, 1971, 1972, 1979/1980, and 1984 had the highest severity. 14 drought events were identified by the SAD method that were consistent with historical records from the Meteorological Disaster Record in China-Yunnan (MDRCY), and 6 events were identified that were not in the MDRCY. Conversely, 4 drought events were recorded in the MDRCY but not identified by the SAD method. These droughts mostly have a short duration and small affected area. It may be related to the threshold selecting and clustering algorithm in drought identification. The SAD method would ignore some mild drought events. Such as the grid with SPI3 greater than − 1 would not be clustered into drought grids.

3.2. Dynamic temporal and spatial characteristics of largest drought events

We selected 6 largest drought events (Table 2) for each decade based on the ranked duration, area, and severity to further analyze the dynamic characteristics of droughts in YP. The drought duration, maximum affected area, and severity of the selected events in the 1960 s, 1970 s, and 1980 s were higher than those in the other decades. The maximum severity was nearly similar, all above 0.9, which

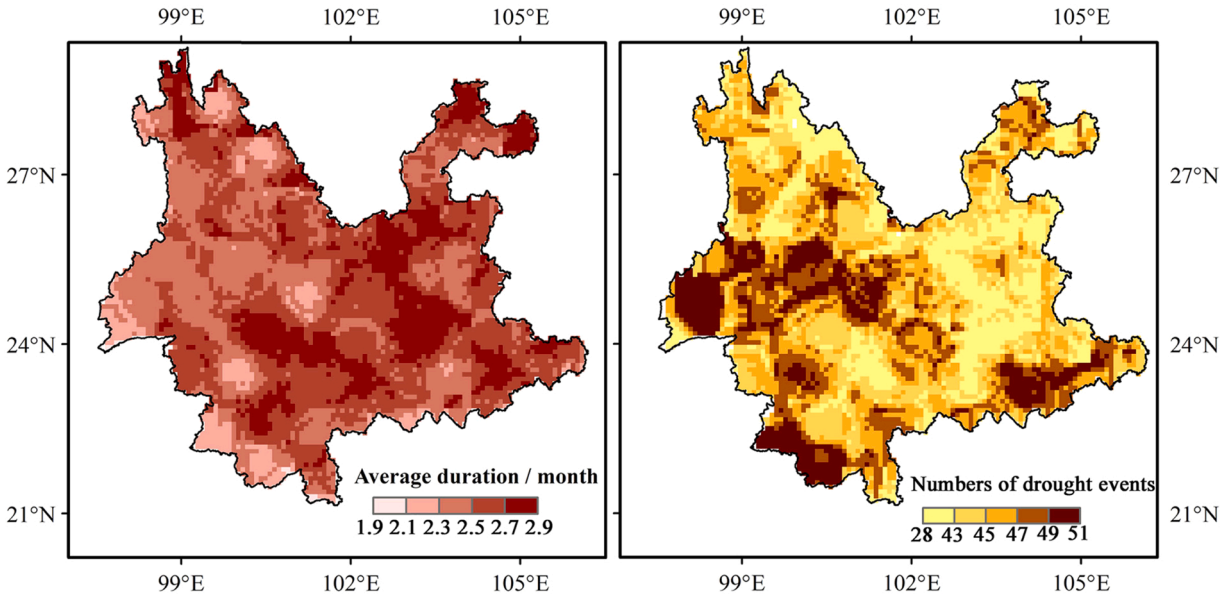

Fig. 3. Spatial distribution of the average duration and number of drought events in YP during 1961–2018.

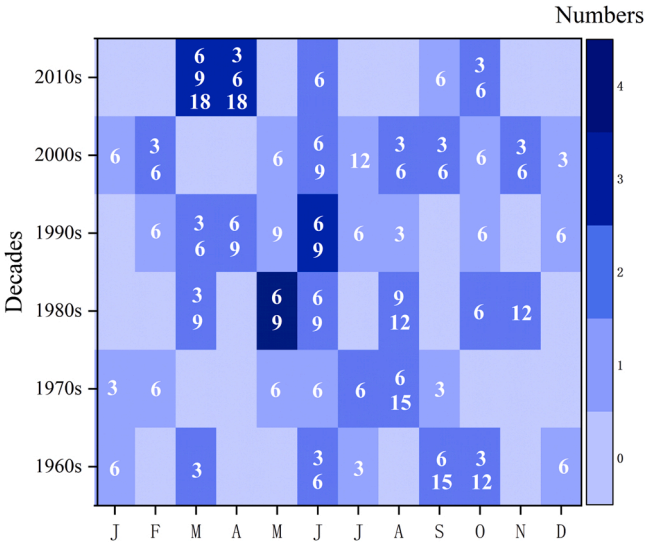

Fig. 4. Decadal-scale statistics of the onset drought events with different durations (3, 6, 9, 12, and 15 months).

Table 1
The duration, maximum affected area, maximum severity of identified drought events, and historical record of drought events in YP during 1960–2000.

Decades	ID	Drought events	Duration (months)	Maximum affected area (%)	Maximum severity (0–1)	Recorded drought year
1960s	4	03/1962–05/1962	3	12.08 (05/1962)	0.93 (04/1962)	√
	*	06/1961–08/1961	3	*	*	√
	18	06/1964–09/1964	4	32.30 (07/1964)	0.95 (06/1964)	×
	28	03/1966–05/1966	3	86.33 (03/1966)	0.92 (05/1966)	√
	35	06/1967–10/1967	5	68.97 (09/1967)	0.99 (06/1967)	√
	45	10/1968–07/1969	10	82.41 (05/1969)	1.00 (10/1968)	√
1970s	59	02/1971–05/1971	4	26.40 (04/1971)	1.00 (02/1971)	×
	*	01/1972–08/1972	8	*	*	√
	73	07/1972–12/1972	6	53.49 (10/1972)	1.00 (11/1972)	×
	*	01/1973–04/1973	4	*	*	√
	80	01/1974–03/1974	3	69.37 (02/1974)	0.99 (01/1974)	×
	97	06/1975–11/1975	6	32.34 (08/1975)	0.98 (11/1975)	√
	107	05/1977–10/1977	6	51.43 (06/1977)	0.99 (06/1977)	√
1980s	123	11/1979–09/1980	11	56.22 (04/1980)	1.00 (11/1979)	√
	143	05/1982–12/1982	8	39.76 (07/1982)	0.99 (10/1982)	√
	147	03/1984–05/1984	3	73.97 (03/1984)	1.00 (05/1984)	√
	166	05/1986–09/1986	5	19.17 (06/1986)	0.99 (09/1986)	√
	184	05/1988–10/1988	6	56.16 (07/1988)	0.99 (10/1988)	√
1990s	199	08/1990–10/1990	3	38.00 (10/1990)	0.93 (08/1990)	×
	205	04/1991–07/1991	4	18.19 (05/1991)	0.98 (06/1991)	×
	*	12/1992–01/1993	2	*	*	√
	216	06/1993–08/1993	3	55.70 (07/1993)	0.94 (08/1993)	√
	223	05/1994–07/1994	3	18.75 (06/1994)	0.94 (07/1994)	√
	254	02/1999–06/1999	5	55.24 (04/1999)	0.95 (06/1999)	√

Note: √: Represents the drought events were recorded in the meteorological disaster record in China-Yunnan; × : Represents the present drought events that have been unrecorded in the meteorological disaster record in China-Yunnan; * : Represents the ID, maximum affected area, and severity of the drought event were not recorded in the meteorological disaster record in China-Yunnan.

is consistent with Fig. 2(d) which shows that the average severity approaches > 0.8 for the largest droughts by area. The most notable drought occurred in the 2010 s (2011–2012), occurring over 18 months and having the highest severity. In terms of the affected area, prominent droughts occurred in the 1960 s, and the maximum affected area covered YP almost entirely.

SAD curves for different durations (3, 6, 9, 12, 15, and 18 months) were plotted to gain further insights into the characteristics of 6 largest droughts (Fig. 5). For the 3-month duration (Fig. 5(a)), the curves of the droughts in the 1960s, 1970s, 2000s, and the 2010s are similar for areas less than 10×10^4 km^2, whose severities were lower than those of the 1980s and 1990s. Meanwhile, the drought in the 1990 s dominated for areas less than 3×10^4 km^2 in terms of severity; however, the 1980s drought dominated as the area increased. For the 6-month duration (Fig. 5(b)), the slope of the curve for the drought in the 1990s rapidly decreases for the area above 8×10^4 km^2, even less than that of the drought in the 2010s, along with an increase in area. In the 1960s, the drought severity was significantly

Table 2
6 largest droughts for each decade.

DroughtID	Duration (months)	Maximum affected area (%)	Maximum Severity (0–1)
03	09/1962–09/1963 (13)	92.10 (01/1963)	0.999 (11/1962)
24	08/1978–09/1979 (14)	75.93 (02/1979)	0.997 (07/1979)
39	03/1987–10/1987 (7)	81.62 (05/1987)	0.999 (06/1987)
47	04/1992–11/1992 (8)	67.91 (08/1992)	0.998 (05/1992)
78	07/2009–05/2010 (11)	86.73 (12/2009)	1.000 (12/2009)
80	04/2011–09/2012 (18)	86.85 (08/2011)	1.000 (07/2011)

lower than that in other decades; however, the drought-affected area was relatively large. For durations of over 15 months (Fig. 5(e) and (f)), there existed only one event which occurred in the 2010s, with the severity and spatial area lower than that of the others. This could have occurred as the average severity over the whole period would likely be lower as the drought developed and receded over a longer period.

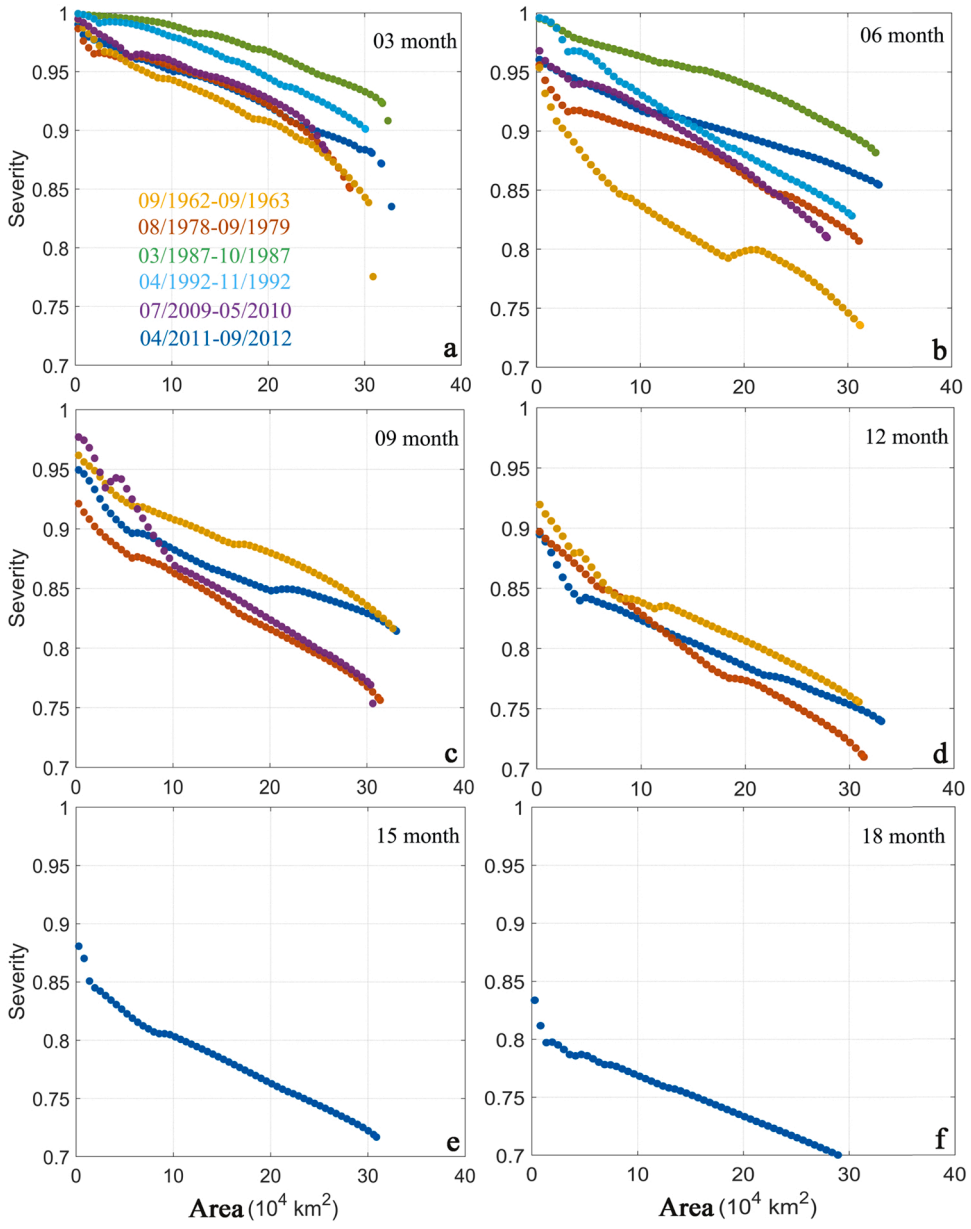

Fig. 5. SAD curves with different durations for 6 largest drought events.

Fig. 6 shows the spatial distribution of the 6 largest droughts in terms of the drought area and severity in the peak month, and also the paths of the drought centers for each month (i.e. the track of the drought center from month to month during the drought duration). The selected peak month was based on a comprehensive index, which was calculated for each month as drought affected area multiplied by the average severity (Wang et al., 2011). This indicates that these drought events had a wide extent, with some covering

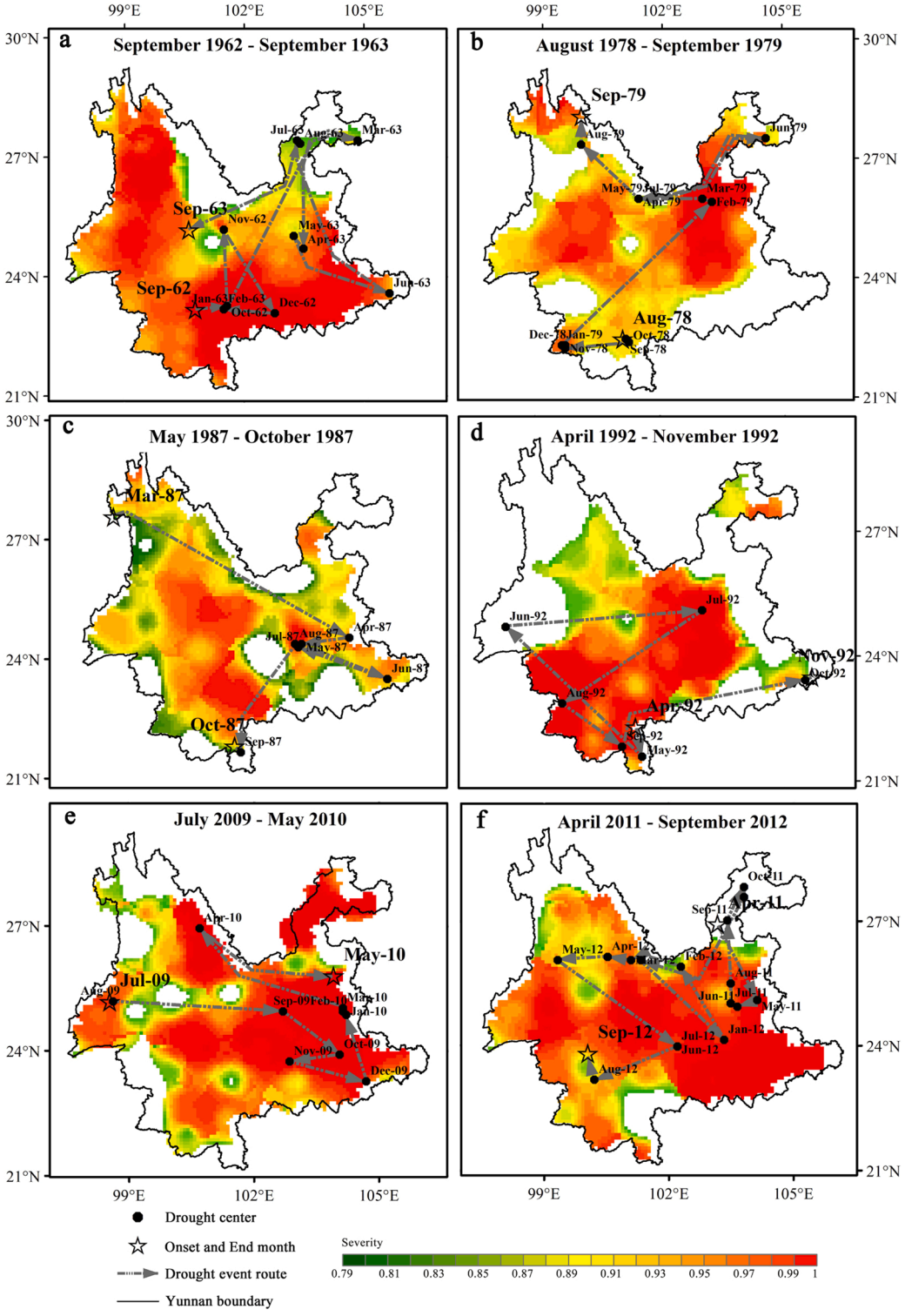

Fig. 6. The shifting paths of drought centers and spatial distribution for the peak month of the droughts for 6 largest drought events.

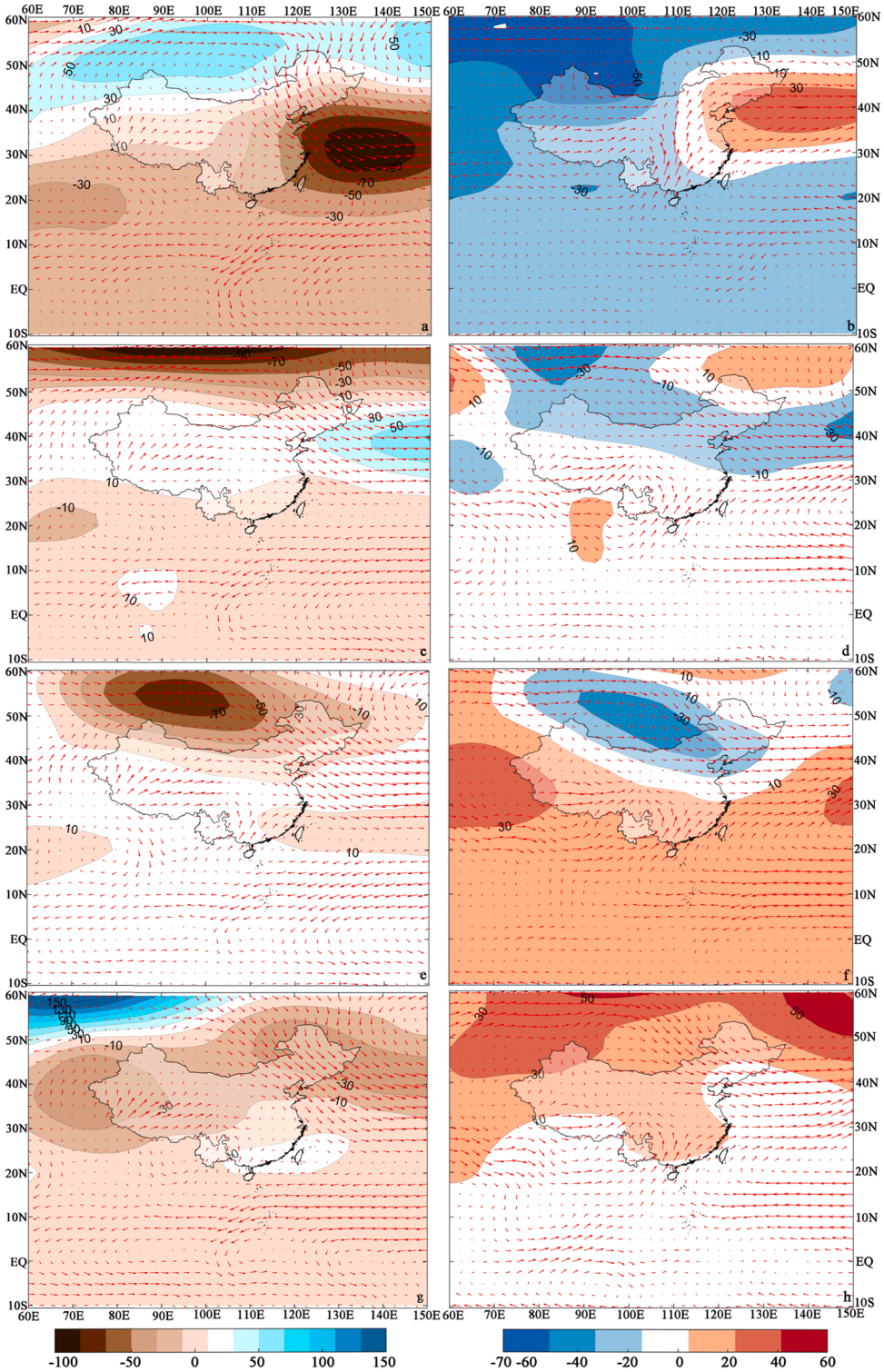

Fig. 7. The geopotential height anomalies at 500 hPa (Shadings denote geopotential height anomalies levels as shown by the color bars; units: gpm) and its winds (red vectors; units: $m \cdot s^{-1}$) at 850 hPa during (a) Winter 1962, (b) Spring 1963, (c) Winter 1978, (d) Spring 1979, (e) Winter 2009, (f) Spring 2010, (g) Winter 2011, and (h) Spring 2012.

YP almost entirely. The paths of the drought centers underwent considerable changes each month. The droughts in the 1960s, 2000s, and 2010s were more severe than the others.

For example, the 1962–1963 drought (Fig. 6(a)) occurred first in the southwest of YP (located in Pu'er City), and it moved toward eastern YP in the subsequent months. The peak month of the drought occurred in Yuxi City; thereafter, the drought faded away in northern YP (Dali City). The 1978–1979 drought (Fig. 6(b)) mainly existed in the southwest of YP in the early period, while it shifted to the northeast of YP in the peak month. The MDRCY recorded that the drought intensified in the Lincang City in February 1979, which severely impacted the growth of crops, such as flue-cured tobacco, spring corn, and rape. From October to December 1979, a continuous drought occurred in autumn and winter in southwest YP, which also severely affected agricultural production. The paths of the droughts identified by the SAD method are generally consistent with the droughts recorded by the MDRCY. The drought events in the 1980s and 1990s (Fig. 6(c and d)) were shorter and less severe; moreover, the drought-affected area was also smaller than that of other drought events.

In particular, this study identified two severe drought events, those of 2009–2010 and 2011–2012, both of which had the longest drought duration (18 and 11 months, respectively). However, Wang et al. (2013) found a 100-year drought in 2009–2012 to be an individual drought event, which differed from our results. This could be related to the different periods and datasets. Both of those droughts were observed to mostly cover YP (Fig. 6(e and f)); also, the drought centers of 2009–2010 for each month were located in eastern YP; however, those of 2011–2012 were located in northeast and northwest YP. Although drought in the peak month (November 2009) had a wide spatial extent, the drought severity in the east was far greater than that in the west.

The results show that drought reached a peak from winter to next spring in these typical drought events. To reveal the influence of large-scale circulation on the shifting path of typical droughts, we further analyzed the wind field at 850 hPa and geopotential height anomalies at 500 hPa in winter and spring. For the August 1978-September 1979 drought, we found that there were significantly negative geopotential height anomalies in the high latitudes and positive geopotential height anomalies on the east and west sides of middle latitudes (Fig. 7(c)). This indicates that westerlies kept a relatively flat state. The difference between positive and negative geopotential height anomalies in the low latitude was not obvious, which was difficult for cold air to move to the south. Baikal Lake displayed negative geopotential height anomalies and the northern Arabian Sea presents positive geopotential height anomalies (Fig. 7(d)). It shows that the weak cold air in the north and the strong subtropical high in the Western Pacific may jointly affect YP drought shifting paths.

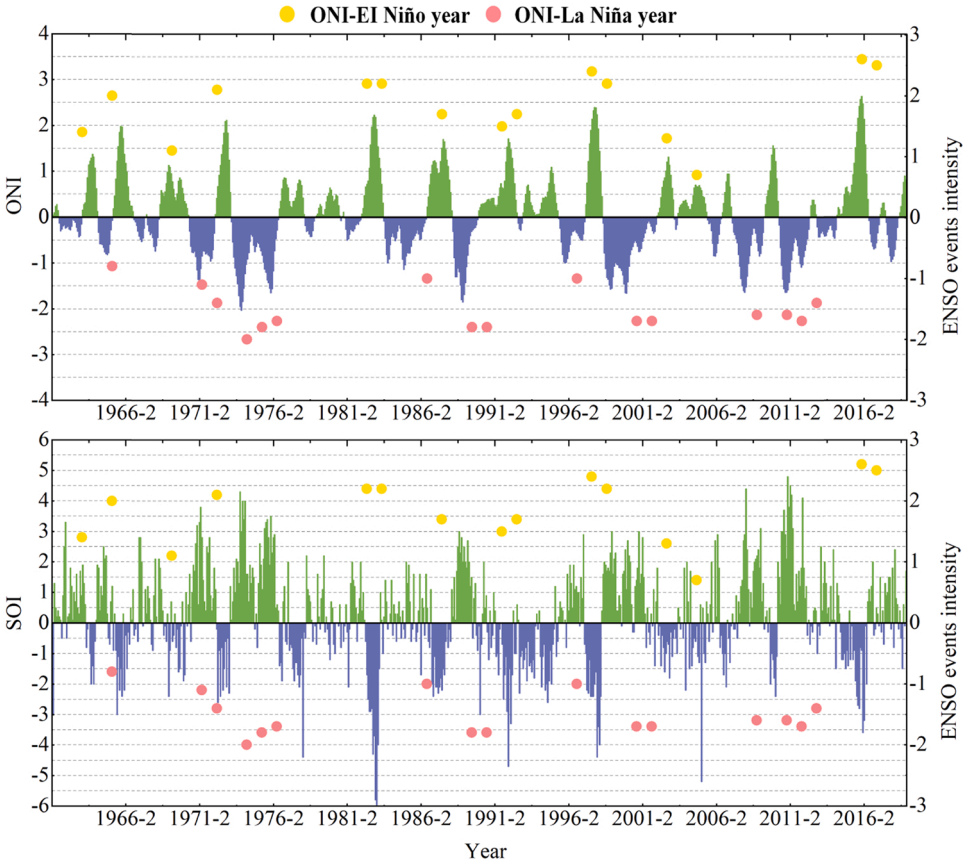

Fig. 8. Temporal series of monthly values for the ONI and SOI. (The ONI-EI Niño year and ONI-La Niña year represent EI Niño period and La Niña period (Table 3) identified by ONI).

There were weak fluctuations in the South Branch trough (Rong et al., 2018; Yang et al., 2012), but the geopotential height anomalies in the Bay of Bengal were not significantly varied (Fig. 7(e)). It indicates that the water vapor in YP in winter contributed less than that of other seasons, which can lead to precipitation reduction. The conclusion is the same as the results of Song et al. (2011), who found that the weak South Branch trough system is the key reason for the reduction of precipitation in YP. In spring (Fig. 7(f)), there were positive geopotential height anomalies over the Bay of Bengal, and the southwest wind on the east side of the Bay of Bengal was weak. Meanwhile, from the wind field at 850 hPa we can find that the water vapor in the southwest reached Sichuan Province and the south of Northwest China, which led to an increase in precipitation over these regions. But the water vapor transport over YP mainly came from the temperate zone north of 20°N, resulting in significantly less precipitation in eastern YP.

The April 2011-September 2012 drought, the negative geopotential height anomaly near Baikal Lake reflects that the pressure ridge was weakened (Fig. 7(g)). Meanwhile, China was controlled by positive geopotential height anomalies in spring 2012 (Fig. 7(h)). The pressure ridge of the Qinghai Tibet plateau developed and controlled YP, which caused the precipitation to continually decrease during this period. In this way, the centers of this drought event involved most areas of YP.

3.3. Correlation and periodicity analysis between droughts and the ENSO

Fig. 8 shows the temporal series of the ONI and SOI, where the various ENSO event intensities are marked. Considering the ENSO events (Table 3), the most intense EI Niño event in the last 6 decades was identified in 2014–2016. The strongest La Niña events were identified in 1973–1974 and 1988–1989. The number of EI Niño events (17 events) was equal to the number of La Niña events during 1961–2018 based on the identification method of the NOAA Earth System Research Laboratory.

To reveal the multi-scale relationships and periodic properties between the climate indices (ONI and SOI) and the SPI3 series, a cross-wavelet analysis was used. The correlation between the ONI and SPI3 in spring (Fig. 9(a)) was observed to be primarily negative with periods of 2–4 year bands during 1964–1972. The phase difference indicated that the change in the ONI was faster than that for SPI3. A noticeably positive correlation with similar period bands was found between the SOI and SPI3 during 1964–1972 (Fig. 10 (a)); moreover, SPI3 was ahead of the SOI. A significant positive correlation existed between the SOI and SPI3 during 4–6 years in summer (Fig. 10 (b)). Fig. 9(d) demonstrated that the significant wavelet power was consistently distributed in the 2–3 year during 1969–1973; 3–6 year during 1982–1990; and 2–4 year during 2008–2014. The phase relationships between the ONI and SPI3 for the periods 1969–1973 and 2008–2014 were prominent in the anti-phase, indicating the negative multi-scale relationships between the two series across YP. The phase of the significant regions (Fig. 10 (d)) was approximately 90°, implying that the SOI led the SPI3 by nearly 3 months. This indicated that the large-scale atmospheric circulation showed strong linkages with the seasonal SPI3; therefore, it strongly influenced the occurrence of drought in YP.

Undoubtedly, precipitation is the most critical meteorological variable affecting drought (Yao et al., 2019). YP droughts are affected by monsoon precipitation and show obvious seasonality (Ding and Gao, 2020). It is easy to form severe drought when the southwest monsoon and the southeast monsoon are relatively weak. Whilst many researchers considered that droughts were linked to global climate variability and had a “lagged response” to the ENSO. The lag period varies depending on different impact factors (Yao et al., 2019; Li et al., 2019).

Here, the correlation coefficients were calculated between the ONI and precipitation in different lag periods (3, 6, 9, and 12 months). The results indicate a correlation between seasonal precipitation and the ONI, which indicates an association between the climate index and the occurrence of droughts in YP. As illustrated in Fig. 11 (a), a negative correlation existed between the ONI of the

Table 3
Identified ENSO events during 1961–2018.

Decades	EI Niño period	Duration (months)	Maximum intensity	La Niña period	Duration (months)	Maximum intensity
1960 s	06/1963–02/1964	9	1.4	05/1964–01/1965	9	-0.8
	05/1965–04/1966	12	2.0			
	10/1968–05/1969	8	1.1			
	08/1969–01/1970	6	0.9			
1970 s	05/1972–03/1973	11	2.1	07/1970–01/1972	19	-1.4
	09/1976–02/1977	6	0.8	05/1973–07/1974	15	-1.8
	09/1977–01/1978	5	0.8	10/1974–04/1976	19	-1.7
1980 s	04/1982–06/1983	15	2.2	09/1983–01/1984	5	-1.0
	09/1986–02/1988	18	1.7	10/1984–08/1985	11	-1.1
				05/1988–05/1989	13	-1.8
1990 s	05/1991–06/1992	14	1.7	08/1995–03/1996	8	-1.0
	09/1994–03/1995	7	1.1	07/1998–12/1999	18	-1.7
	05/1997–05/1998	13	2.4			
2000 s	06/2002–02/2003	9	1.3	01/2000–02/2001	14	-1.7
	07/2004–02/2005	8	0.7	11/2005–03/2006	5	-0.8
	09/2006–01/2007	5	0.9	07/2007–06/2008	12	-1.6
	07/2009–03/2010	9	1.6	11/2008–03/2009	5	-0.8
				06/2010–05/2011	12	-1.7
	11/2014–05/2016	19	2.6	07/2011–03/2012	9	-1.1
				08/2016–12/2016	5	-0.7
				10/2017–03/2018	6	-1.0

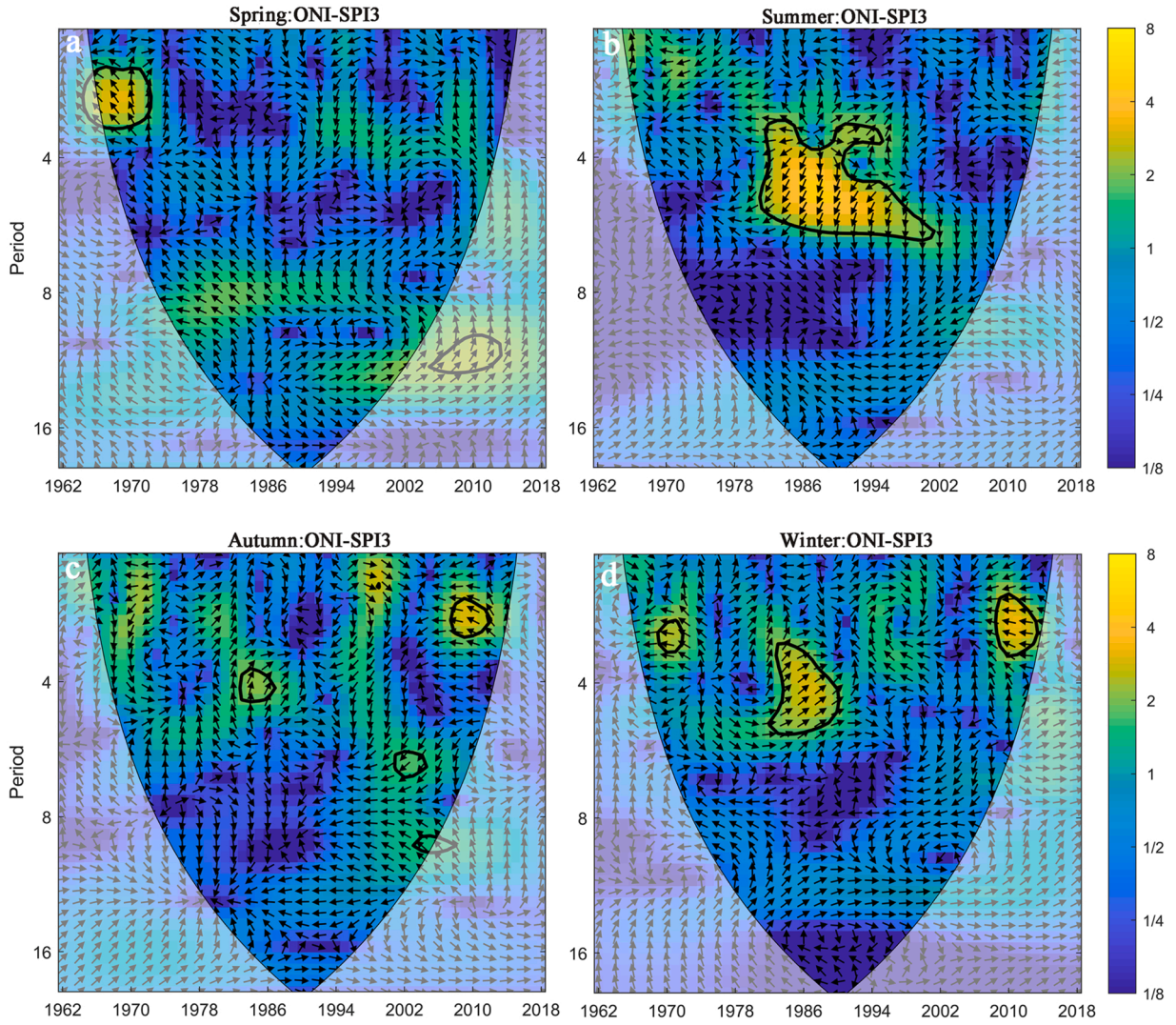

Fig. 9. The cross-wavelet transform between four seasons based on the ONI and SPI3 series. The Yellow noise within the thick line represents that 5% confidence level and the arrow indicates the relative phase relationship (negative correlation points to the left and positive correlation points to the right; the downward arrow indicates that SPI3 is ahead of ONI, and the upward arrow indicates ONI is ahead of SPI3). (For interpretation of the references to colour in this figure, the reader is referred to the web version of this article.)

early four seasons and the later spring precipitation in YP from the mid-1980 s to the lat-1990 s, which indicated that spring precipitation was less in the El Niño years, especially in 1987–1990, 1993–1996 and 1999–2001. It can be verified from the identified drought events that 40% of them occurred in spring from the mid-1980 s to the mid-1990 s. The lag period between the ONI and precipitation (Fig. 12 (a)) was mostly 3 months before 1990 s, and it was prolonged to 6, 9, and 12 months in 2000 s. This change may be related to the interdecadal shift of the ENSO that occurred around 1999/2000, in which the forecasted SSTA always lagged observed for several months (McPhaden, 2012; Hu et al., 2013, 2016, 2017c, 2020).

A positive correlation was seen in the 2010 s, such that spring precipitation was less in the La Niña year of this period. The lag period reached 12 months. This study also identified 6 droughts that occurred in spring, accounting for 54% of the total events in the 2010 s the 2011–2012 drought has the largest severity and longest duration with the drought affected area covering YP almost entirely. A significant positive correlation was found between the ONI of the early summer, autumn, and later winter precipitation (Fig. 11 (d)) during the 1980 s and 2000 s, which indicates that the winter precipitation was less in the same period of the La Niña year. The lag period in winter (Fig. 12 (d)) was longer than other seasons from 1960 s to 1990 s but shortened in 2000 s. El Niño and La Niña events have significant effects on autumn precipitation, but the effect decade was varied. The effect of the El Niño event was mainly in the 1970–1980 s, and the La Niña event was in the 1990–2000 s. The lag period of the two events for autumn precipitation was relatively long, reaching 12 months. This long lag period is exacerbated by the multiple factors, such as the response of soil moisture, natural vegetation, hydrological and atmospheric systems to drought conditions, that commonly occur in the response of climatic

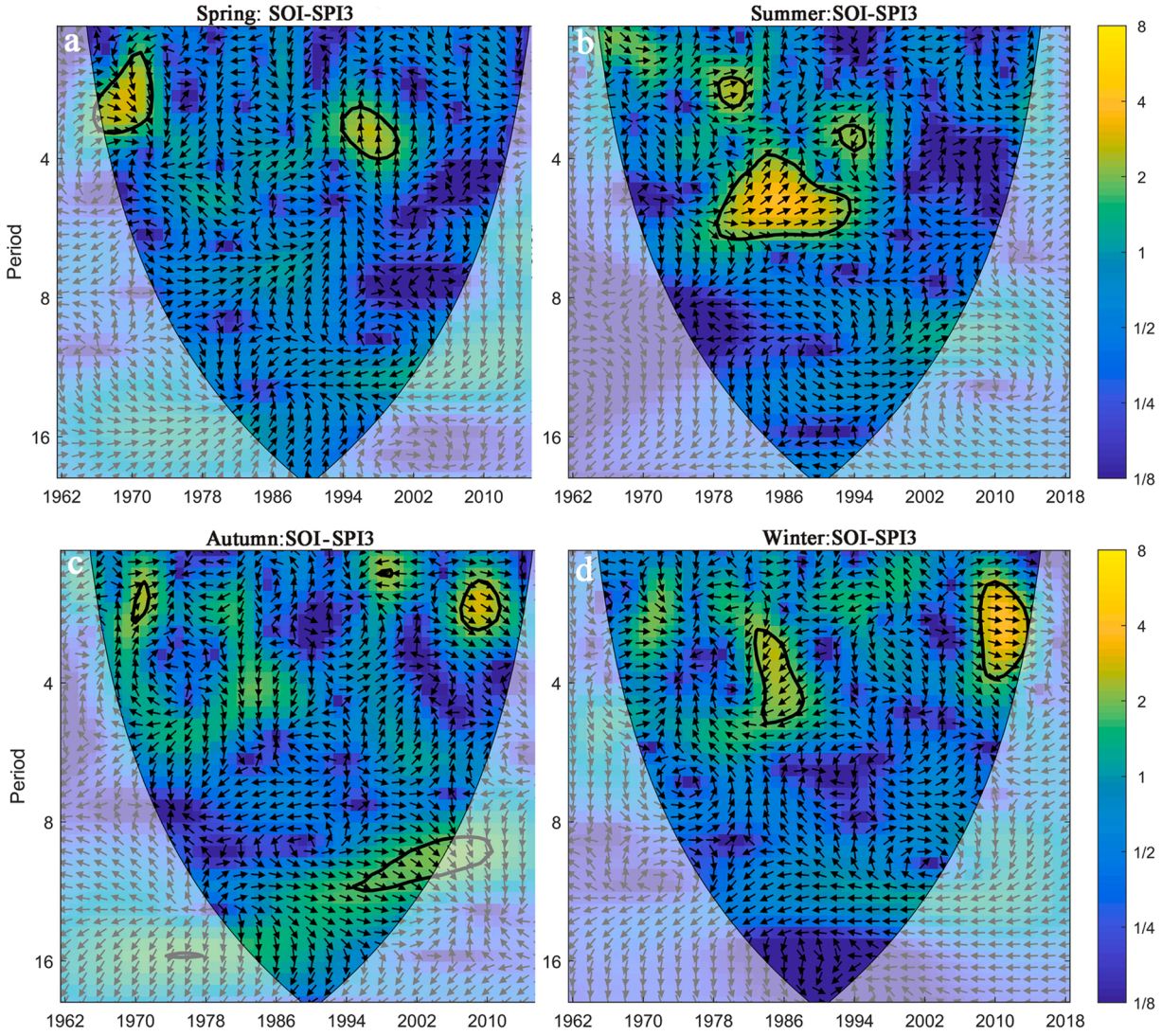

Fig. 10. The cross-wavelet transform between four seasons based on the SOI and SPI3 series.

conditions to atmospheric circulation events (Ji and Peters, 2003; Patel et al., 2007; Khan et al., 2008; Quiring and Ganesh, 2010).

4. Discussion

Drought identification has always been a hot issue and considering its spatial and temporal dimensions can help improve drought monitoring (Diaz et al., 2019; Wen et al., 2020). Results of identification of drought location and characteristics using the SAD method in YP are discussed in this section. It is obvious that the average drought severity and area have risen steadily over the past 58 years, and droughts were most likely to occur from January to May. The location where drought occurred severely and frequently varies during the study period, among which the east and south of YP are the most prone to drought. These results have been mentioned in other studies (Table 4). For example, Yu et al. (2020), Yang et al. (2019), and Li et al. (2015a), (2015b) indicated that droughts significantly became more frequent with the extension of the timescale, especially after 2000 s Cheng et al. (2020) found that the central, southern, and northeastern parts of YP experienced the longest drought duration and the higher drought severity occurred in the eastern and southwestern parts of YP. Yu et al. (2013) indicated that March to May is more prone to drought on the temporal distribution, which is in accordance with our results. 6 largest drought events were identified, including those of 1962–1963, 1978–1979, 1987, 1992, 2009–2010, and 2011–2012. These severe droughts were recorded by MDRCY. In addition, the spatial distribution of the peak month of the largest droughts was generally consistent with the recorded regions (Wen and Liu, 2006; Mao et al., 2009, 2010, 2011, 2012).

These findings demonstrate that the SAD method can help identify droughts, whilst also describing the joint drought characteristics, including drought severity, frequency, and spatial distribution. But the choice of thresholds for the SAD method directly affects

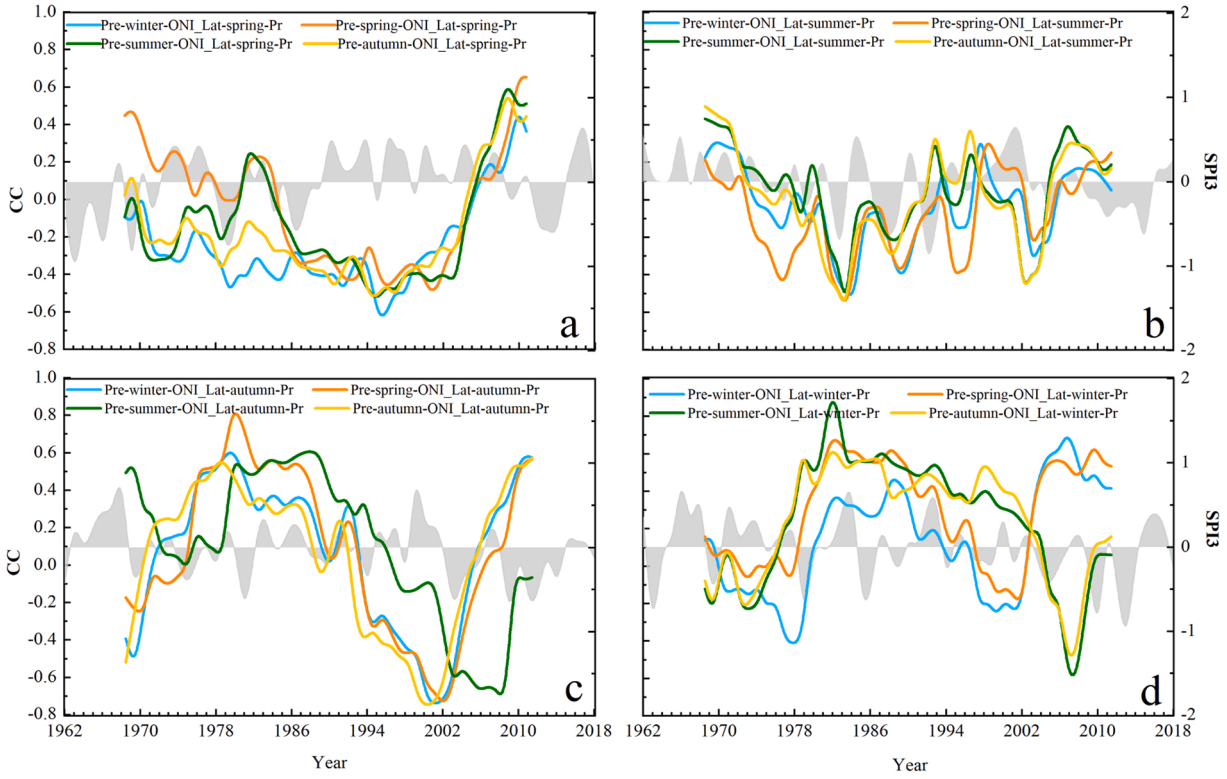

Fig. 11. The sliding correlation coefficients (CC) between the ONI and precipitation in different lagging periods (3, 6, 9, and 12 months). The grey area represents the SPI3 series.

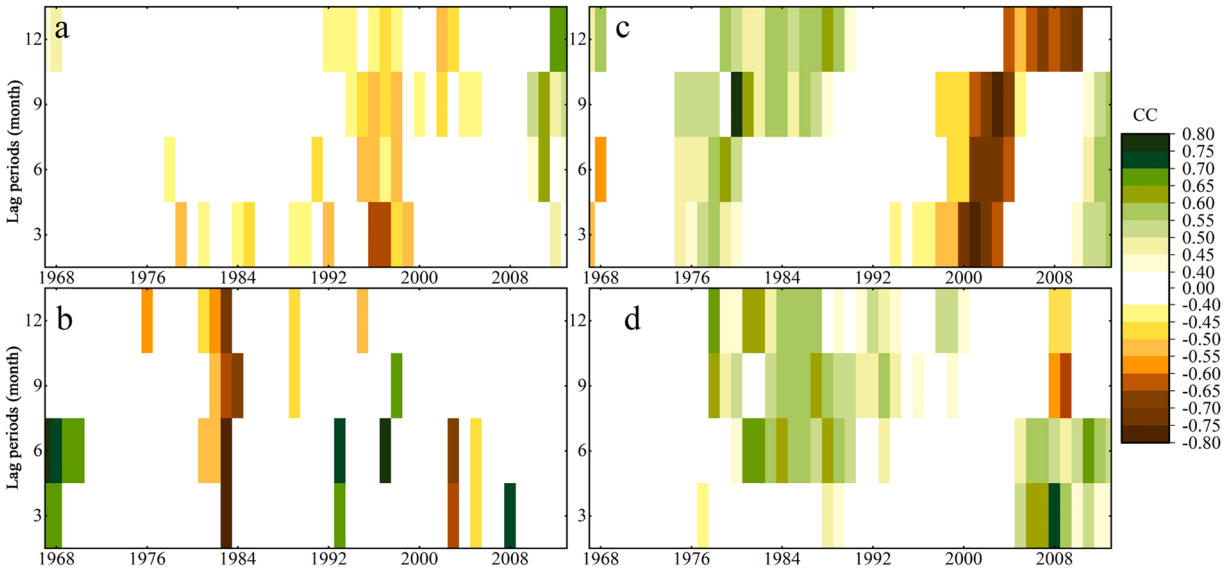

Fig. 12. Significant lagged correlation (CC exceeding +/- 0.4) between the seasonal (Spring (a), Summer (b), Autumn (c), and Winter (d)) ONI and precipitation in different lagging periods (3, 6, 9, and 12 months).

the number of identified drought events (Andreadis et al., 2005). Wang et al. (2011) found that drought events might be repeated in different months when selecting different thresholds. Sheffield et al. (2009) found that a smaller threshold could shrink drought clusters to a few grid cells and persist for many years. To avoid this situation, a minimum threshold (6000 km^2) was set to identify the drought events based on the results, wherein the suitable minimum area threshold was ~1.5% of the study area (Wang et al., 2011).

Table 4
Comparison of drought location and characteristics.

Study period	Evaluation Index	Drought location	Characteristics			Data sources
			frequency	area	duration	
1960–2013	RDI	Southwest and Southeast	*	*	↑	Cheng et al. (2020)
2009–2018	CI	The whole YP	↑	↑	*	Yu et al. (2020)
1960–2010	Pa and TRCI	Central and Northeast	↑	↑	*	Zhang et al. (2015)
1961–2015	SPEI	West and East	↑	↑	*	Li et al. (2019)
1969–2018	SPI and SPEI	North and East	↑	↑	↑	Yang et al. (2019)
1950–2010	CI	The whole YP	↑	*	↑	Yu et al. (2013)
1982–2012	SPEI	*	↑	*	*	Li et al. (2015a), (2015b)

Note: ↑: Represents an increasing trend; * : Represents this characteristic is not specifically mentioned in the paper.

Meanwhile, Sheffield et al. (2009) also found that the drought frequency between decades can be revealed by using different thresholds to identify drought events. Therefore, the number of drought events could be further assessed using different thresholds or different regions in YP to understand the sensitivity of the approach.

This study explored the correlation and periodicity between climate indices (ONI and SOI) and SPI3. The results found that the ONI had a stronger correlation with SPI3 in YP. A significantly negative correlation was identified with periods of 2–4 year bands in 1964–1972, which is consistent with the results of Cheng et al. (2020). A sliding correlation method was used to analyze the impact of ONI on seasonal precipitation and their lag periods. Results demonstrated that El Niño and La Niña years were associated with seasonal droughts in YP; moreover, droughts could occur in both El Niño and La Niña years, but the lag period varied in different seasons. For example, the lag period of the effect of El Niño on spring precipitation was about 3 months before the 1990 s, but it was prolonged to 12 months from the 1990–2000 s. In winter, the negative correlation trend for different lag periods (3, 6, 9, and 12 months) was similar from the 1980 s to the mid-1990 s which indicated that the La Niña event had a significant effect on the later winter precipitation, resulting in the decrease of later winter precipitation. Significantly, droughts were more likely to occur in spring during El Niño years and in winter during La Niña years. Quantification of drought lag period is helpful to formulate drought measures to deal with the drought occurrence.

Researchers have pointed out that the number and density of meteorological stations may be one of the factors affecting the precipitation interpolation (Sinha et al., 2006; Villarini and Krajewski, 2008; Zhang et al., 2011; Shope and Ram, 2015). Topographic elements such as elevation, aspect, and slope also affect the interpolation results. However, limited by the data availability, we used 22 meteorological stations data to explore YP drought characteristics. The results have been verified by using recorded drought events in MDRCY, and many previous studies on droughts in Yunnan Province have used a similar number of meteorological stations (Yu et al., 2020; Cheng et al., 2020; Zhang et al., 2015; Yang et al., 2019). Furthermore, not only ENSO events were responsible for droughts in YP during our study period, but other drivers also need to be identified (Yao et al., 2019). Various meteorological factors, such as relative humidity, temperature, and wind speed need to be considered in future research on droughts in YP. Meanwhile, human activities, such as land cover change, water resource management, irrigation water use, and groundwater withdrawal could also impact droughts (Wang and Meng, 2013; He et al., 2017; Sun et al., 2019; Yang et al., 2020a, 2020b). These factors affecting the evolution and dynamic changes of droughts need further exploration.

5. Conclusion

This study explored the spatial and temporal dynamics of drought characteristics in YP and quantified the correlation and periodicity between droughts and ENSO were explored to reveal the possible factors influencing YP droughts. The result shows that 74 drought events were identified during 1961–2018 in YP. The month of onset of a drought mainly occurred in summer, while the end month mostly occurred in autumn. The 2011–2012 drought was the most prominent with the highest duration and severity; furthermore, the peak month occurred in September 2011, with a drought area of ~86.85% of the region of YP. The drought center paths of the largest drought events underwent significant changes across YP with time.

The correlation between the SPI3 and large-scale climate indices (ONI and SOI) showed notable seasonal characteristics, which indicate that YP droughts could be related to the El Niño (La Niña) events. The relationship between precipitation and the ONI demonstrates that droughts in spring mainly occurred in both El Niño and La Niña years during the 1980s and the 2010s, and the lag period was about 3 months in the 1980s, but it was prolonged to 12 months in the 2010s, and those in winter mainly occurred in La Niña years during the 1990s and the 2000s with a lag period of up to 12 months.

At present, dynamic identification of drought occurrence and processes is crucial to drought monitoring and early warning. The present study helps improve the drought monitoring mechanism and provides a potential reference for identifying drought evolution processes, which can reduce the economic losses caused by drought in Yunnan province.

Funding

This work was supported by the General Project of the National Natural Science Foundation of China (Grant No. 52079036 and U2243203).

CRediT authorship contribution statement

Linyan Zhang: Methodology, Data curation, Calculation, Formal analysis, Writing – original draft, Writing – review & editing. **Xiaoli Yang:** Conceptualization, Supervision, Validation. **Liliang Ren:** Supervision, Validation. **Justin Sheffield:** Validation, Writing – review & editing. **Linqi Zhang:** Writing – review & editing. **Shanshui Yuan:** Writing – review & editing. **Mengru Zhang:** Data curation.

Declaration of Competing Interest

The authors declare the following financial interests/personal relationships which may be considered as potential competing interests: Xiaoli Yang reports financial support was provided by the General Project of the National Natural Science Foundation of China.

Acknowledgments

The authors would like to thank the Chinese Meteorological Data Sharing Service and the NOAA Earth System Research Laboratory for providing study datasets. We thank associate professor Xiaogang He, the National University of Singapore, for providing the idea and framework of this article.

Appendix A. Supporting information

Supplementary data associated with this article can be found in the online version at doi:10.1016/j.ejrh.2022.101128.

References

Andreadis, K.M., et al., 2005. Twentieth-century drought in the conterminous United States. J. Hydrometeorol. 6, 985–1001. https://doi.org/10.1175/JHM450.1.
Caloiero, T., et al., 2018. Drought analysis in Europe and in the Mediterranean Basin using the Standardized Precipitation Index. Water 10, 1043. https://doi.org/10.3390/w10081043.
Cao, J., Hu, J., Tao, Y., 2012. An index for the interface between the Indian summer monsoon and the East Asian summer monsoon. J. Geophys. Res-Atmos. 117, D18108. https://doi.org/10.1029/2012JD017841.
Chen, S., Yuan, X., 2021. CMIP6 projects less frequent seasonal soil moisture droughts over China in response to different warming levels (https://iopscience.iop.org/article/). Environ. Res. Lett. 16, 044053. https://doi.org/10.1088/1748-9326/abe782.
Cheng, Q., et al., 2020. Spatiotemporal variations of drought in the Yunnan-Guizhou Plateau, southwest China, during 1960-2013 and their association with large-scale circulations and historical records. Ecol. Indic. 112, 106041 https://doi.org/10.1016/j.ecolind.2019.106041.
Diaz, V., et al., 2019. Characterisation of the dynamics of past droughts. Sci. Total Environ. 718, 134588 https://doi.org/10.1016/j.scitotenv.2019.134588.
Ding, T., Gao, H., 2020. The record-breaking extreme drought in Yunnan Province, Southwest China during spring-early summer of 2019 and possible causes. J. Meteorol. Res. 34, 997–1012. https://doi.org/10.1007/s13351-020-0032-8.
Giovannettone, J., Zhang, Y., 2019. Identifying strong signals between low-frequency climate oscillations and annual precipitation using correlation analysis. Int. J. Climatol. 39, 4883–4894. https://doi.org/10.1002/joc.6107.
Hao, C., Zhang, J., Yao, F., 2017. Multivariate drought frequency estimation using copula method in Southwest China. Theor. Appl. Climatol. 127, 977–991. https://doi.org/10.1007/s00704-015-1678-5.
Hao, Z., AghaKouchak, A., 2013. Multivariate standardized drought index: a parametric multi-index model. Adv. Water Resour. 57, 12–18. https://doi.org/10.1016/j.advwatres.2013.03.009.
Hao, Z., Singh, V.P., 2015. Drought characterization from a multivariate perspective: a review. J. Hydrol. (Amst.) 527, 668–678. https://doi.org/10.1016/j.jhydrol.2015.05.031.
He, X., et al., 2017. Intensification of hydrological drought in California by human water management. Geophys. Res. Lett. 44, 1777–1785. https://doi.org/10.1002/2016GL071665.
He, X., et al., 2020. A Global drought and dlood catalogue from 1950 to 2016. B. Am. Meteorol. Soc. 101, E508–E535. https://doi.org/10.1175/BAMS-D-18-0269.1.
Hu, Z.Z., et al., 2013. Weakened interannual variability in the tropical Pacific Ocean after 2000. J. Clim. 26, 2601–2613. https://doi.org/10.1175/JCLI-D-12-00265.1.
Hu, Z.Z., et al., 2016. Spatial distribution and the interdecadal change of leading modes of heat budget of the mixed-layer in the tropical Pacific and the association with ENSO. Clim. Dyn. 46, 1753–1768. https://doi.org/10.1007/s00382-015-2672-4.
Hu, Z.Z., et al., 2017c. On the shortening of the lead time of ocean warm water volume to ENSO SST after 2000. Sci. Rep. 7, 4294 https://doi.org/650 10.1038/s41598-017-04566-z.
Hu, Z.Z., et al., 2020. The interdecadal shift of ENSO properties in 1999/2000: a review. J. Clim. 33, 4441–4462. https://doi.org/10.1175/JCLI-D-19-0316.1.
Hudgins, L.H., 1993. Wavelet transforms and atmospheric turbulence. Phys. Rev. Lett. 71, 3279. https://doi.org/10.1103/PhysRevLett.71.3279.
Ji, L., Peters, A.J., 2003. Assessing vegetation response to drought in the northern Great Plains using vegetation and drought indices. Remote Sens. Environ. 87, 85–98. https://doi.org/10.1016/S0034-4257(03)00174-3.
Khan, S., Gabriel, H.F., Rana, T., 2008. Standard Precipitation Index to track drought and assess impact of rainfall on watertables in irrigation areas. Irrig. Drain. Syst. 22, 159–177. https://doi.org/10.1007/s10795-008-9049-3.
Li, X., 2015b. Use of the Standardized Precipitation Evapotranspiration Index (SPEI) to characterize the drying trend in southwest China from 1982–2012. Remote Sens. 7, 10917–10937. https://doi.org/10.3390/rs70810917.
Li, Y., et al., 2015a. Variability of extreme precipitation over Yunnan Province, China 1960-2012. Int. J. Climatol. 35, 245–258. https://doi.org/10.1002/joc.3977.
Li, Y., et al., 2019. Drought variability at various timescales over Yunnan Province, China: 1961-2015. Theor. Appl. Climatol. 138, 743–757. https://doi.org/10.1007/s00704-019-02859-z.
Li, Y., Liu, X.D., 2011. Features of the extremely severe drought in the east of southwest China and anomalies of atmospheric circulation in summer 2006. Acta Metall. Sin. -Engl. 25, 176–187. https://doi.org/10.1007/s13351-011-0025-8.
Liu, H., et al., 2013. Drought evaluation and reconstruction based on a hydrologic model and remote sensing. J. Tsinghua Univ. (Sci. Technol.) 53, 613–617. https://doi.org/10.16511/j.cnki.qhdxxb.2013.05.003.
Liu, L., et al., 2019. Revisiting assessments of ecosystem drought recovery. Environ. Res. Lett. 14, 11402811. https://doi.org/10.1088/1748-9326/ab4c61.

Liu, M., 2014. Is southwestern China experiencing more frequent precipitation extremes? Environ. Res. Lett. 9, 064002 https://doi.org/10.1088/1748–9326/9/6/064002.
Liu, X., et al., 2015. Regionalization and spatiotemporal variation of drought in China based on Standardized Precipitation Evapotranspiration Index (1961–2013). Adv. Meteor. 2015, 1–18. https://doi.org/10.1155/2015/950262.
Liu, Z., Zhang, X., Fang, R., 2018. Multi-scale linkages of winter drought variability to ENSO and the arctic oscillation: a case study in Shaanxi, north China. Atmos. Res. 200, 117–125. https://doi.org/10.1016/j.atmosres.2017.10.012.
Ma, B., et al., 2020. Conditional distribution selection for SPEI-daily and its revealed meteorological drought characteristics in China from 1961 to 2017. Atmos. Res. 246, 105108 https://doi.org/10.1016/j.atmosres.2020.105108.
Ma, Z.F., et al., 2013. Observed climate changes in southwest China during 1961-2010. Adv. Clim. Chang. Res. 4, 30–40. https://doi.org/10.3724/SP.J.1248.2013.030.
Mao, Y., Xu, X., Wang, C., 2009. China Meteorological Disaster Yearbook. China Meteorological Press,, Beijing.
Mao, Y., Xu, X., Wang, C., 2010. China Meteorological Disaster Yearbook. China Meteorological Press,, Beijing.
Mao, Y., Xu, X., Wang, C., 2011. China Meteorological Disaster Yearbook. China Meteorological Press,, Beijing.
Mao, Y., Xu, X., Wang, C., 2012. China Meteorological Disaster Yearbook. China Meteorological Press,, Beijing.
Mckee, T.B., et al., 1993. The relationship of drought frequency and duration to time scales. Eighth Conference on Applied Climatology. American Meteorological Society,, Anaheim, CA, pp. 179–186.
McPhaden, M.J., 2012. A 21st century shift in the relationship between ENSO SST and warm water volume anomalies. Geophys. Res. Lett. 39, L09706. https://doi.org/10.1029/2012GL051826.
de Oliveira-Júnior, J.F., 2018. Drought severity based on the SPI index and its relation to the ENSO and PDO climatic variability modes in the regions north and northwest of the State of Rio de Janeiro-Brazil. Atmos. Res. 212, 91–105. https://doi.org/10.1016/j.atmosres.2018.04.022.
Patel, N.R., Chopra, P., Dadhwal, V.K., 2007. Analyzing spatial patterns of meteorological drought using Standardized Precipitation Index. Meteorol. Appl. 14, 329–336. https://doi.org/10.1002/met.33.
Philander, S.G.H., 1983. El Niño Southern Oscillation phenomena. Nature 302, 295–301. https://doi.org/10.1038/302295a0.
Quiring, S.M., Ganesh, S., 2010. Evaluating the utility of the Vegetation Condition Index (VCI) for monitoring meteorological drought in Texas. Agric. . Meteorol. 150, 330–339. https://doi.org/10.1016/j.agrformet.2009.11.015.
Rong, Y.S., et al., 2018. Analysis on characteristics and causes of persistent meteorological and hydrological drought in Yunnan from 2009 to 2014. Water Resour. Prot. 34, 22–29 https://doi.org/CNKI:SUN:SZYB.0.2018-03-004.
Scaini, A., 2015. SMOS-derived soil moisture anomalies and drought indices: a comparative analysis using in situ measurements. Hydrol. Process. 29, 373–383. https://doi.org/10.1002/hyp.10150.
Shao, D., 2018. Drought characteristics over China during 1980-2015. Int. J. Climatol. 38, 3532–3545. https://doi.org/10.1002/joc.5515.
Sheffield, J., 2009. Global and continental drought in the second half of the Twentieth Century: severity-area-duration analysis and temporal variability of large-scale events. J. Clim. 22, 1962–1981. https://doi.org/10.1175/2008JCLI2722.1.
Shope, C.L., Ram, M.G., 2015. Modeling spatiotemporal precipitation: effects of density, interpolation, and land use distribution. Adv. Meteorol. 2015, 1–16. https://doi.org/10.1155/2015/174196.
Sinha, S.K., Narkhedkar, S.G., Mitra, A.K., 2006. Bares objective analysis scheme of daily rainfall over Maharashtra (India) on a Mesoscale grid. Atmosfera 19, 109–126.
Song, et al., 2011. A further study of causes of the severe drought in Yunnan Province during the 2009/2010 winter. Chin. J. Atmos. Scicnces 35, 1009–1019 https://doi.org/CNKI:SUN:DQXK.0.2011-06-003.
Song, L., et al., 2019. Divergent vegetation responses to extreme spring and summer droughts in Southwestern China. Agr. For. Meteorol. 279, 107703 https://doi.org/10.1016/j.agrformet.2019.107703.
Su, B., 2021. Insight from CMIP6 SSP-RCP scenarios for future drought characteristics in China. Atmos. Res. 25, 105375 https://doi.org/10.1016/j.atmosres.2020.105375.
Sun, S., et al., 2019. Revisiting the evolution of the 2009-2011 meteorological drought over Southwest China. J. Hydrol. 568, 385–402. https://doi.org/10.1016/j.jhydrol.2018.10.071.
Tayfur, G., 2021. Discrepancy precipitation index for monitoring meteorological drought. J. Hydrol. 597, 126174 https://doi.org/10.1016/j.jhydrol.2021.126174.
Torrence, C., Compo, G.P., 1998. A practical guide to wavelet analysis. B. Am. Meteorol. Soc. 79, 61–78. https://doi.org/10.1175/1520-0477(1998)079<0061:APGTWA>2.0.CO;2.
Torrence, C., Webster, P.J., 1999. Interdecadal changes in the ENSO-monsoon system. J. Clim. 12, 2679–2690. https://doi.org/10.1175/1520-0442(1999)012<2679:ICITEM>2.0.CO;2.
Torres-Valcarcela, A.R., 2018. Teleconnections between ENSO and rainfall and drought in Puerto Rico. Int. J. Climatol. 381, E1190–E1204. https://doi.org/10.1002/joc.5444.
Udmale, P., et al., 2020. A statistical approach towards defining national-scale meteorological droughts in India using crop data. Environ. Res. Lett. 15, 0940909. https://doi.org/10.1088/1748-9326/abacfa.
Villarini, G., Krajewski, W.F., 2008. Empirically-based modeling of spatial sampling uncertainties associated with rainfall measurements by rain gauges. Adv. Water Resour. 31, 1015–1023. https://doi.org/10.1016/j.advwatres.2008.04.007.
Wanders, N., et al., 2017. Forecasting the hydroclimatic signature of the 2015/16 El Nino event on the Western United States. J. Hydrometeorol. 18, 177–186. https://doi.org/10.1175/JHM-D-16-0230.1.
Wang, A., Lettenmaier, D.P., Sheffield, J., 2011. Soil moisture drought in China, 1950-2006. J. Clim. 24, 3257–3271. https://doi.org/10.1175/2011JCLI3733.1.
Wang, J., Meng, Y., 2013. An analysis of the drought in Yunnan, China, from a perspective of society drought severity. Nat. Hazards 67, 431–458. https://doi.org/10.1007/s11069-013-0572-7.
Wang, S., Huang, J., Yuan, X., 2021. Attribution of 2019 extreme spring-early summer hot drought over Yunnan in Southwestern China. B. Am. Meteorol. Soc. 102, S91–S96. https://doi.org/10.1175/BAMS-D-20-0121.1.
Wang, Z., et al., 2017. Increasing drought has been observed by SPEI_pm in Southwest China during 1962–2012. Theor. Appl. Climatol. 133, 23–38. https://doi.org/10.1007/s00704-017-2152-3.
Wen, K., Liu, J., 2006. China Meteorological Disaster (Yunnan volume). China Meteorological Press, Beijing.
Wen, X., et al., 2020. Construction of 3D drought structures of meteorological drought events and their spatio-temporal evolution characteristics. J. Hydrol. 590, 125539 https://doi.org/10.1016/j.jhydrol.2020.125539.
Yadav, R.K., Ramu, D.A., Dimri, A.P., 2013. On the relationship between ENSO patterns and winter precipitation over North and Central India. Glob. Plant. Change 107, 50–58. https://doi.org/10.1016/j.gloplacha.2013.04.006.
Yang, C., 2019. Spatial and temporal evolution characteristics of drought in Yunnan Province from 1969 to 2018 based on SPI/SPEI. Water Air. Soil. Pollut. 230, 1–13. https://doi.org/10.1007/s11270-019-4287-6.
Yang, H., 2012. Cause of the severe drought in Yunnan Province during winter of 2009. Clim. Environ. Res. 17, 315–326. https://doi.org/10.3878/j.issn.1006-9585.2011.101134.
Yang, X., et al., 2020a. Spatial and temporal characterization of drought events in China using the Severity-Area-Duration method. Water 12, 2301. https://doi.org/10.3390/w12010230.
Yang, X., et al., 2020b. Contrasting influences of human activities on hydrological drought regimes over China based on high-resolution simulations. Water Resour. Res. 56 https://doi.org/10.1029/2019WR025843.
Yao, J., et al., 2019. Identification of drought events and correlations with large-scale Ocean-Atmospheric Patterns of variability: a case study in Xinjiang, China. Atmosphere 10, 942. https://doi.org/10.3390/atmos10020094.

Yu, W., 2013. Analysis on spatial and temporal characteristics drought of Yunnan Province. Acta Ecol. Sin. 33, 317–324. https://doi.org/10.1016/j.chnaes.2013.09.004.

Yu, Y., et al., 2020. Drought monitoring in Yunnan Province based on a TRMM precipitation product. Nat. Hazards 104, 2369–2387. https://doi.org/10.1007/s11069-020-04276-2.

Zambrano Mera, Y.E., et al., 2018. Linking El Niño Southern Oscillation for early drought detection in tropical climates: The Ecuadorian coast. Sci. Total. Environ. 643, 193–207. https://doi.org/10.1016/j.scitotenv.2018.06.160.

Zhai, J., et al., 2016. Intensity-area-duration analysis of droughts in China 1960–2013. Clim. Dynam. 48, 151–168. https://doi.org/10.1007/s00382-016-3066-y.

Zhan, W., 2020. Projected seasonal changes in large-scale global precipitation and temperature extremes based on the CMIP5 ensemble. J. Clim. 33, 5651–5671. https://doi.org/10.1175/JCLI-D-19-0311.1.

Zhang, D., et al., 2015. Copula-based risk assessment of drought in Yunnan Province, China. Nat. Hazards 75, 2199–2220. https://doi.org/10.1007/s11069-014-1419-6.

Zhang, G.P., et al., 2011. The influence of gauge density on the interpolation of critical and antecedent effective precipitation that triggered the debris flow. Geogr. Res. 30, 1237–1243 https://doi.org/CNKI:SUN:DLYJ.0.2011-07-009.

Zhang, Y., et al., 2021. Drought monitoring based on a new combined remote sensing index across the transitional area between humid and arid regions in China. Atmos. Res. 264, 105850 https://doi.org/10.1016/j.atmosres.2021.105850.

Zhou, L., et al., 2021. The influence of ENSO and MJO on drought in different ecological geographic regions in China. Remote Sens. 13, 8755. https://doi.org/10.3390/rs13050875.